

Two-level Quantum Walkers on Directed Graphs II: An Application to qRAM

Ryo Asaka*, Kazumitsu Sakai[†] and Ryoko Yahagi[‡]

*Department of Physics, Tokyo University of Science,
Kagurazaka 1-3, Shinjuku-ku, Tokyo 162-8601, Japan*

April 19, 2022

Abstract

This is the second paper in a series of two. Using a multi-particle continuous-time quantum walk with two internal states, which has been formulated in the first paper (arXiv:2112.08119), we physically implement a quantum random access memory (qRAM). Data with address information are dual-rail encoded into quantum walkers. The walkers pass through perfect binary trees to access the designated memory cells and copy the data stored in the cells. A roundabout gate allocated at each node serves as a router to move the walker from the parent node to one of two child nodes, depending on the internal state of the walker. In this process, the address information is sequentially encoded into the internal states so that the walkers are adequately delivered to the target cells. The present qRAM, which processes 2^n m -qubit data, is implemented in a quantum circuit of depth $O(n \log(n + m))$ and requires $O(n + m)$ qubit resources. This is more efficient than the conventional bucket-brigade qRAM that requires $O(n^2 + nm)$ steps and $O(2^n + m)$ qubit resources for processing. Moreover, since the walkers are not entangled with any device on the binary trees, the cost of maintaining coherence can be reduced. Notably, by simply passing quantum walkers through binary trees, data can be automatically extracted in a quantum superposition state. In other words, any time-dependent control is not required.

1 Introduction

This is the second paper in a series of two in which we consider a multi-particle continuous-time quantum walk with two internal states. In the present paper, we propose a physical implementation of a quantum random access memory (qRAM), using some devices developed in the first paper [1], in which an architecture of universal quantum computation using the quantum walk has been provided.

*E-mail: hello.ryoasaka@gmail.com

[†]E-mail: k.sakai@rs.tus.ac.jp

[‡]E-mail: yahagi@rs.tus.ac.jp

A number of quantum algorithms exploiting quantum mechanical effects have been proposed to achieve significant speedups over their classical analogs [2]. Algorithms for quantum phase estimation [3, 4], quantum amplitude amplification [5–8], and quantum Hamiltonian simulation [9–18] are the most notable, and are used as subroutines in, for example, Shor’s algorithm for factorizing large integers [3] and Grover’s algorithm for searching unsorted databases [7]. However, one should be careful about claiming that quantum algorithms are superior to classical counterparts in some cases. As an example, let us take the search problem of finding a particular item in an unstructured set consisting of N items. Grover’s algorithm incorporates the process of accessing and querying the database as an oracle (a black box that answers yes or no) and completes the search with only $O(\sqrt{N})$ oracle queries, achieving a quadratic speedup over classical exhaustive search. In practice, however, the oracle subroutines, i.e., converting data into a quantum superposition state, accessing and reading them, maybe a cumbersome overhead that offsets the quantum speedup [19]. Namely, reducing a cost to the oracle is crucial for applications of quantum computation to search problems, Hamiltonian simulations and machine learning for big data [20–38].

A quantum random access memory (qRAM) was introduced as a quantum counterpart of a RAM, promising to efficiently access data and convert them into superposition states [39, 40]. Conceptually, a qRAM is a quantum device comprising the following three principal schemes: (i) a routing scheme to access the specified memory cells whose addresses are given by an n -qubit superposition state

$$\sum_a |a\rangle_A = \sum_{\{a_j\}} |a_{n-1} \cdots a_0\rangle_A \in (\mathbb{C}^2)^{\otimes n}, \quad a \in \mathbb{Z}_{\geq 0}, \quad a_j \in \{0, 1\} \quad (0 \leq j \leq n-1), \quad (1.1)$$

(ii) a querying scheme to read the classical information $x^{(a)} \in \mathbb{Z}_{\geq 0}$ stored in the a th cell¹ and (iii) an output scheme to retrieve the data in an m -qubit superposition state $\sum_a |x^{(a)}\rangle_D$. Here, the subscripts A and D stand for the quantum versions of an address register and a data register, respectively. Explicitly, a qRAM is defined as a function

$$\text{qRAM: } \sum_a |a\rangle_A |0\rangle_D \mapsto \sum_a |a\rangle_A |x^{(a)}\rangle_D. \quad (1.2)$$

Giovannetti, Lloyd and Maccone (GLM) proposed a remarkable qRAM architecture using the so-called bucket-brigade routing scheme [39, 40]. The GLM architecture is defined on a perfect binary tree with depth n on which $N = 2^n$ data are stored in the memory cells placed on the leaves of the binary tree (see Fig. 1). Each node in the tree is equipped with a qutrit with three energy labeled *wait*, *left*, and *right*, and all the qutrits are initially in the *wait* state. The qutrit acts as a router: the value $a_{n-1-\ell} \in \{0, 1\}$ ($0 \leq \ell \leq n-1$) in the address register (1.1) is delivered to one of the 2^ℓ nodes at the ℓ th level of the binary tree, and if $a_{n-1-\ell} = 0$ (resp. $a_{n-1-\ell} = 1$), activates the qutrit from *wait* to *left* (resp. *right*) to route the subsequent $a_{n-2-\ell}$ to one of the two child nodes. After $O(n^2) = O(\log^2 N)$ steps, a unique route is assigned from the root to the specified memory cell, as schematically depicted in Fig. 1. A quantum bus then arrives at the cell through the assigned route, the data stored in the cell is coherently loaded onto the bus, and the bus loaded with the data returns to the root via the route it came from. Finally, reverting the activated qutrits to

¹A qRAM can also process the quantum information where $|x^{(a)}\rangle$ consists of a superposition of states. See Sec. 5. For the moment, however, we restrict ourselves to the classical case for convenience.

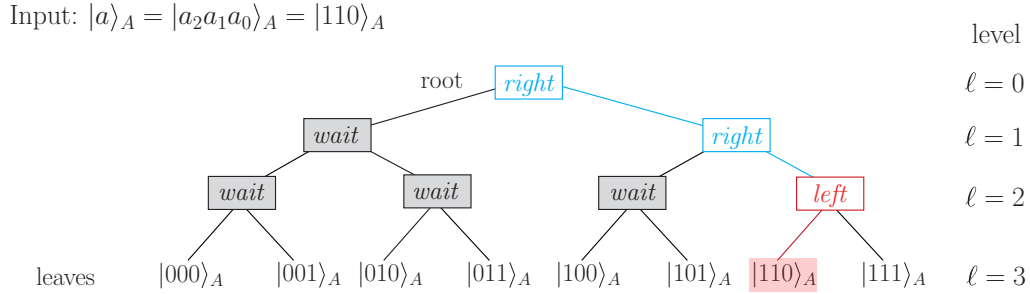


Figure 1: The GLM bucket-brigade scheme defined on a binary tree with depth $n = 3$. A qutrit is installed at each node to route to the specified memory cells. For instance, to route to the cell at address $|110\rangle_A$, the three qutrits must be activated from *wait* to *left/right*.

wait, sequentially from the last level, yields output in the r.h.s of (1.1). For each memory call, the overall computational cost and qubit resources required to process $N = 2^n$ m -qubit data are $O(n^2 + nm)$ and $O(2^n + m)$, respectively.

It is worth noting that the number of qutrits to be activated is only $O(n)$, which drastically reduces a cost of maintaining the quantum coherence compared to the fan-out scheme (most commonly used in a classical RAM) that activates $O(2^n)$ qutrits. In fact, a high resilience of the bucket-brigade qRAM to generic noise has been recently proved in [41]. The GLM qRAM has been improved and is realized efficiently by quantum circuits as in [42–44]. Some experimental implementations have also been proposed in [40, 45–48].

More recently, the authors of the present paper have provided a novel qRAM algorithm that works on a perfect binary tree but does not require entanglement with any quantum device on the nodes [49]. In this sense, this algorithm promises to reduce the cost of maintaining quantum coherence compared to the bucket-brigade scheme, but its implementation has remained open until now. The purpose of this paper is to physically implement this qRAM algorithm using a multi-particle continuous-time quantum walk with two internal states.

Our qRAM architecture is roughly sketched as follows. First, quantum information is dual-rail encoded into quantum walkers moving on parallel paths; a single-qubit data is represented by the presence of a walker on one of the two parallel paths. Namely, the arbitrary m -qubit data associated with n -qubit address information is represented by a set of $n+m$ quantum walkers traveling on half of $2(n+m)$ paths. Second, each walker possesses two internal states (e.g., the spin-up and down states of an electron). Depending on the internal state, the roundabout gate allocated at each node of the binary trees passes the walker to one of the two child nodes. The address information is sequentially encoded into the internal states so that the set of walkers is properly delivered to the designated memory cells. Finally, the data in the cell is copied by simply changing the positions of the walkers in the data register. The set of the walkers carrying the data is retrieved by the reverse operation of the routing scheme.

In the above implementation, the roundabout gate can be actually realized by the scattering of the walker from a directed graph [1]. The encoder, which converts the positional information of the path traveled by the specified walkers into the internal states of the walkers, is implemented by a combination of roundabout gates and single-qubit gates acting on

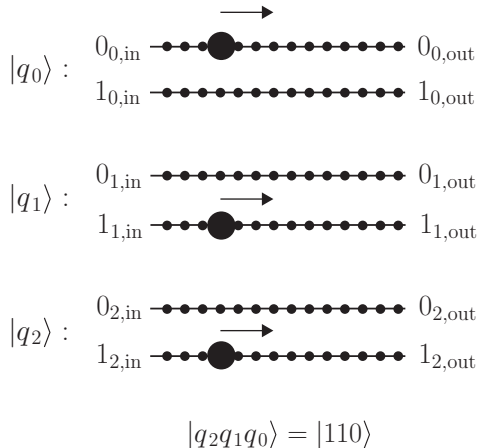


Figure 2: A dual-rail encoding of the state $|q_2q_1q_0\rangle = |110\rangle$.

the internal state of the walkers. The main advantages of our architecture are as follows. (i) The processing is fully parallelized without using any ancilla qubit, and can access and retrieve the m -qubit data associated with n -qubit address information in $O(n \log(n + m))$ steps. The qubit resources necessary for the processing is $O(n + m)$. (ii) The walkers are not entangled with any device on the binary trees, thus reducing the cost of maintaining the quantum coherence. (iii) It does not require any time-dependent control: the qRAM process is automatically achieved by just passing the walkers through binary trees. (iv) Using the model developed in the first paper [1], it is possible to design a unified universal quantum computer that is compatible with the qRAM developed in this paper.

The rest of this paper is outlined as follows. Sec. 2 describes the general setup and gives an overview of our qRAM architecture. Some devices developed in the first paper [1], which are required in the present paper, are also summarized. A physical implementation of the qRAM is provided in Sec. 3. In Sec. 4, an alternative qRAM scheme that transforms a trivial state into a superposition of information stored in the specified memory cells:

$$\widetilde{\text{qRAM}}: |0\rangle_A |0\rangle_D \mapsto \sum_a |a\rangle_A |x^{(a)}\rangle_D \quad (1.3)$$

(cf. (1.2)) is proposed. The last section is devoted to the summary and discussion, where we briefly explain how to extract *quantum* information (i.e. information in quantum superposition) in the designated cells instead of classical information.

2 Preliminaries

This section gives an overview of the qRAM architecture, which is a physical realization of the algorithm developed in [49]. The architecture uses some quantum gates implemented by multi-particle continuous-time quantum walks [1].

2.1 Setup and layout of the qRAM

Our qRAM architecture employs a dual-rail encoding in which data and address information are represented as the positions of the paths the quantum walkers moving; a single-qubit

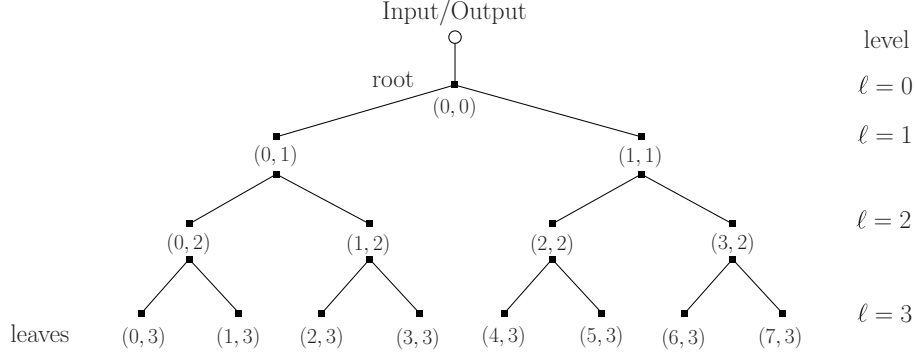


Figure 3: A perfect binary tree with depth $n = 3$. At level ℓ ($0 \leq \ell \leq n$) of the binary tree, the w th node counting from the left is labeled as (w, ℓ) ($0 \leq w \leq 2^\ell - 1$; $0 \leq \ell \leq n$). Each node (w, ℓ) has two child nodes $(2w, \ell + 1)$ (left child) and $(2w + 1, \ell + 1)$ (right child) for $0 \leq \ell \leq n - 1$. The input/output terminal is connected to the root node $(0, 0)$ by a path.

state $|q_j\rangle \in \mathbb{C}^2$ is expressed by the presence of a quantum walker in one of two parallel paths:

$$|q_j\rangle = \delta_{q_j,0}|2j\rangle_p + \delta_{q_j,1}|2j+1\rangle_p \quad (0 \leq j \leq n+m-1), \quad (2.1)$$

where $|2j\rangle_p \in \mathbb{C}^2$ (resp. $|2j+1\rangle_p \in \mathbb{C}^2$) indicates that a walker is moving on the $(2j)$ th (resp. $(2j+1)$ th) path). Correspondingly, an $(n+m)$ -qubit state is given by

$$|q_{n+m-1} \cdots q_0\rangle = |q_{n+m-1}\rangle \otimes \cdots \otimes |q_0\rangle = \bigotimes_{j=0}^{n+m-1} (\delta_{q_j,0}|2j\rangle_p + \delta_{q_j,1}|2j+1\rangle_p) \in (\mathbb{C}^2)^{\otimes(n+m)}. \quad (2.2)$$

Fig. 2 shows an example of a dual-rail encoded state. For our purposes, we assign the first n qubits and the remaining m qubits to the address and data registers, respectively:

$$\begin{aligned} |a\rangle_A &= |a_{n-1} \cdots a_0\rangle_A = |a_{n-1}\rangle_{A_{n-1}} \otimes \cdots \otimes |a_0\rangle_{A_0} = |q_{n-1} \cdots q_0\rangle \in (\mathbb{C}^2)^{\otimes n}, \\ |x^{(a)}\rangle_D &= |x_{m-1}^{(a)} \cdots x_0^{(a)}\rangle_D = |x_{m-1}^{(a)}\rangle_{D_{m-1}} \otimes \cdots \otimes |x_0^{(a)}\rangle_{D_0} = |q_{n+m-1} \cdots q_n\rangle \in (\mathbb{C}^2)^{\otimes m}. \end{aligned} \quad (2.3)$$

The $(n+m)$ quantum walkers (in superposition) access the specified memory cell(s) through half of the $2(n+m)$ parallel paths and retrieve the data stored in the cell(s). To this end, we prepare $2(n+m)$ parallel sheets on each of which two perfect binary trees of depth n are arranged so that the 2^n memory cells are sandwiched between the two sets of 2^n leaves, as schematically shown in Fig. 4. (See also Fig. 3 as a detailed description of a perfect binary tree.) A set of $n+m$ walkers (possibly in superposition) at input (resp. output) terminals of the first (resp. second) binary trees corresponds to the input (resp. output) state. Let (w, ℓ) ($0 \leq w \leq 2^\ell - 1$; $0 \leq \ell \leq n$) be the w th node from the left at the ℓ th level of the perfect binary tree, and let $|w, \ell\rangle_B \in \mathbb{C}^{2^{n+1}-1}$ denote that a set of $n+m$ walkers (called a “bus”) is moving toward the node (w, ℓ) from its parent node (the parent node for the root node $(0, 0)$ denotes the input/output terminal (see Fig. 3)). Namely, the bus that passes between these two nodes, carrying m -qubit data $|x^{(a)}\rangle_D$ associated with an n -qubit address $|a\rangle_A$, is represented as $|a\rangle_A |w, \ell\rangle_B |x^{(a)}\rangle_D$.

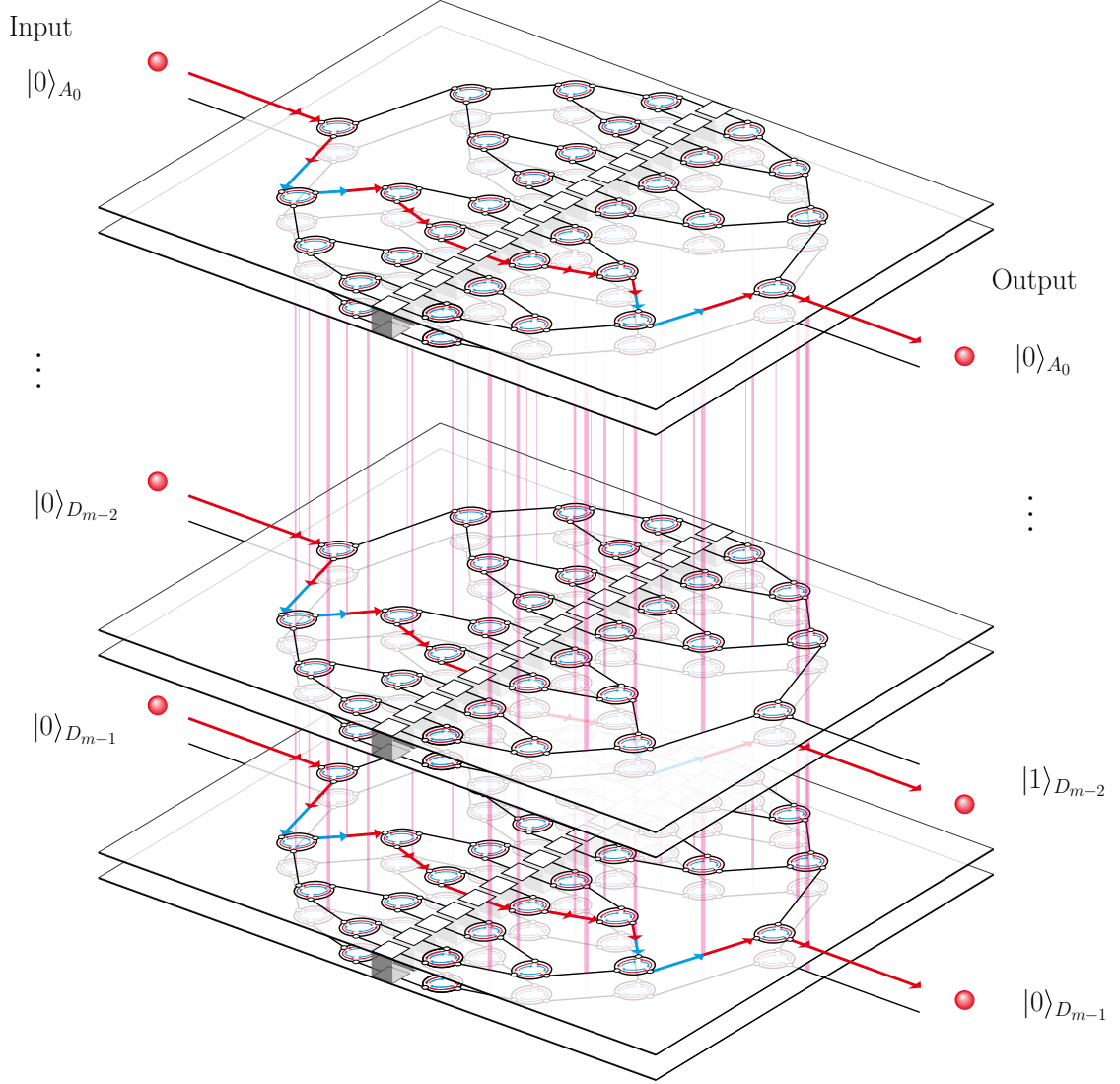


Figure 4: An overview of the current qRAM architecture. Due to the dual-rail encoding (see (2.1), (2.2) and also Fig. 2), the architecture is designed on $2(n + m)$ sheets. Each sheet has two perfect binary trees of depth n (cf. Fig. 3), with their 2×2^n leaves sandwiching the 2^n memory cells. The $n + m$ red quantum walkers at the left back (resp. right front) represent the input (resp. output) state. In the routing scheme, the roundabout gate is set up at each node of the trees so that it passes a red walker (resp. blue walker) to the left (resp. right) child node. The address information $|a_{n-1-\ell}\rangle_{A_{n-1-\ell}}$ is encoded in the internal state of all the $n + m$ walkers as $\otimes_{j=0}^{n+m-1} |a_{n-1-\ell}\rangle_{C_j}$ while they move to the node (w, ℓ) ($0 \leq w \leq 2^\ell - 1$; $0 \leq \ell \leq n - 1$) from its parent node (the parent node for the root node $(0, 0)$ denotes the input terminal). This process can be accomplished by the device $\mathcal{E}_{(w, \ell)}$ intersecting perpendicular to the paths between two levels $\ell - 1$ and ℓ ($0 \leq \ell \leq n - 1$) ($\ell = -1$ denotes the input terminals). The data $x^{(a)}$ stored in the memory cell at address a is loaded to the walkers arriving at the cell. By reversing the routing scheme, the walkers loaded with the data (in superposition) are retrieved as the output.

All the $(n + m)$ quantum walkers possess two internal states (e.g., the spin-up and down states of an electron). Let $|c\rangle_{C_j} \in \mathbb{C}^2$ ($c \in \{0, 1\}$, $0 \leq j \leq n + m - 1$) be the internal state of the j th walker, and we call the walker with $|0\rangle_{C_j}$ and $|1\rangle_{C_j}$ a “red walker” and a “blue walker”, respectively. In principle, we assume that the internal states are initialized to be red $|0\rangle_{C_j}$ ($0 \leq j \leq n + m - 1$) before processes. All the walkers at the input/output terminals are colored red ($|0\rangle_C := \otimes_{j=0}^{n+m-1} |0\rangle_{C_j} \in (\mathbb{C}^2)^{\otimes(n+m)}$), and just before or just after passing through the nodes, all they are colored red or blue ($|2^{n+m} - 1\rangle_C := \otimes_{j=0}^{n+m-1} |1\rangle_{C_j} \in (\mathbb{C}^2)^{\otimes(n+m)}$) according to the address information (1.1). The address information is temporarily encoded in the internal states by a unitary gate $\mathcal{E}_{(w,\ell)}$ that intersects perpendicular to the paths between two levels $\ell - 1$ and ℓ ($0 \leq \ell \leq n - 1$) ($\ell = -1$ denotes the input terminals), as shown in Fig. 4. (See the next section for more details about $\mathcal{E}_{(w,\ell)}$.) A roundabout gate is set up at each node to move a red walker (resp. blue walker) to the left child node (resp. right child node) in the routing scheme, and do exactly the opposite in the output scheme. The data stored in the memory cells are loaded to the walkers in the data register, which is simply realized by changing their positions, as described in the subsequent section. The walkers loaded with the data are retrieved in the output scheme, which is accomplished by reversing the routing scheme. That is a layout of our qRAM given by a function

$$\begin{aligned} \text{qRAM: } (\mathbb{C}^2)^{\otimes\{2(n+m)+\log_2(2^{n+1}-1)\}} &\xrightarrow{\Psi} (\mathbb{C}^2)^{\otimes\{2(n+m)+\log_2(2^{n+1}-1)\}} \\ \sum_{a \in \mathcal{A}} |a\rangle_A |0, 0\rangle_B |0\rangle_C |0\rangle_D &\longmapsto \sum_{a \in \mathcal{A}} |a\rangle_A |0, 0\rangle_B |0\rangle_C |x^{(a)}\rangle_D, \end{aligned} \quad (2.4)$$

where $\mathcal{A} \subset \{0, \dots, 2^n - 1\}$ denotes the set of the addresses of the specified memory cells.

2.2 Quantum gates

Next, we briefly introduce several elementary quantum gates developed in the previous paper [1] that are necessary for the design of the current qRAM architecture.

(a) Single-qubit gates Arbitrary single-qubit gates are universally realized by a combination of roundabout gates, and rotation gates acting on the internal states of the walker.

The roundabout gate serves as a router that moves a walker either clockwise or counterclockwise from one path to the next according to the internal state of the walker:

$$\begin{aligned} U_R^{(l)} &= |0\rangle\langle 0|_{C_j} U_R + |1\rangle\langle 1|_{C_j} U_R^\dagger, \quad U_R^{(r)} = U_R^{(l)\dagger}, \\ U_R &= \sum_{k,l=0}^2 \delta_{l,k+1} |jl\rangle\langle jk|_P \quad (k, l \in \mathbb{Z}/3\mathbb{Z} = \{0, 1, 2\}). \end{aligned} \quad (2.5)$$

Here, $U_R^{(l)}$ (resp. $U_R^{(r)}$) is a unitary operator that moves a red walker (a walker with the internal state $|0\rangle_{C_j}$) (resp. blue walker (a walker with $|1\rangle_{C_j}$)) clockwise (resp. counterclockwise) to

the next path. Graphically, it is represented as

The diagram shows two roundabout gates, $U_R^{(l)}$ and $U_R^{(r)}$. Each gate consists of a central node j_0 at the top, and two side nodes j_1 and j_2 . Two circular paths, one red and one blue, connect the nodes. In $U_R^{(l)}$, the red path goes from j_0 to j_1 and back to j_0 , while the blue path goes from j_0 to j_2 and back to j_0 . In $U_R^{(r)}$, the red path goes from j_0 to j_2 and back to j_0 , while the blue path goes from j_0 to j_1 and back to j_0 .

$$U_R^{(l)} = \text{Diagram} \quad U_R^{(r)} = \text{Diagram} \quad (2.6)$$

For example, the motion of a red/blue walker that enters the $U_R^{(l)}$ or $U_R^{(r)}$ gate from path j_0 is graphically given

Four diagrams illustrate the motion of a walker entering a roundabout gate from the top node j_0 . In the first two diagrams, a red walker enters from j_0 and exits from j_1 (left) or j_2 (right). In the last two diagrams, a blue walker enters from j_0 and exits from j_1 (left) or j_2 (right).

$$\text{Diagram 1} \quad \text{Diagram 2} \quad \text{Diagram 3} \quad \text{Diagram 4} \quad (2.7)$$

Physically the roundabout gate can be implemented by a single-particle scattering from a directed graph as shown in Sec. 3 in [1].

Let us pictorially denote a quantum gate U_{C_j} acting on the internal state $|c\rangle_{C_j}$ of the j th quantum walker as

A cylinder representing a quantum gate U_{C_j} . An arrow labeled "in" enters from the left, and an arrow labeled "out" exits from the right. The input state is $|c\rangle_{C_j}$ and the output state is $U_{C_j}|c\rangle_{C_j}$.

$$\text{Diagram} \quad (2.8)$$

An arbitrary single-qubit gate U_{C_j} is universally realized by $U_{C_j} = e^{i\theta_0} R_z(\theta_1) R_y(\theta_2) R_z(\theta_3)$ ($\theta_k \in \mathbb{R}$ ($k = 0, 1, 2, 3$)) [2, 50], where $R_y(\theta) := e^{-i\theta Y/2}$ (resp. $R_z(\theta) := e^{-i\theta Z/2}$) is the operator that rotates the Bloch vector around the y -axis (z -axis) by a given angle θ . For example, the Pauli-X gate is represented as $X_{C_j} = R_y(\pi)_{C_j}$ whose action on the states $|0\rangle_{C_j}$ and $|1\rangle_{C_j}$ are graphically represented as

Two diagrams show the Pauli-X gate X_{C_j} . The first diagram shows a red dot (state $|0\rangle_{C_j}$) entering from the left and a blue dot (state $|1\rangle_{C_j}$) exiting from the right. The second diagram shows a blue dot (state $|1\rangle_{C_j}$) entering from the left and a red dot (state $|0\rangle_{C_j}$) exiting from the right.

$$\text{Diagram 1} \quad \text{Diagram 2} \quad (2.9)$$

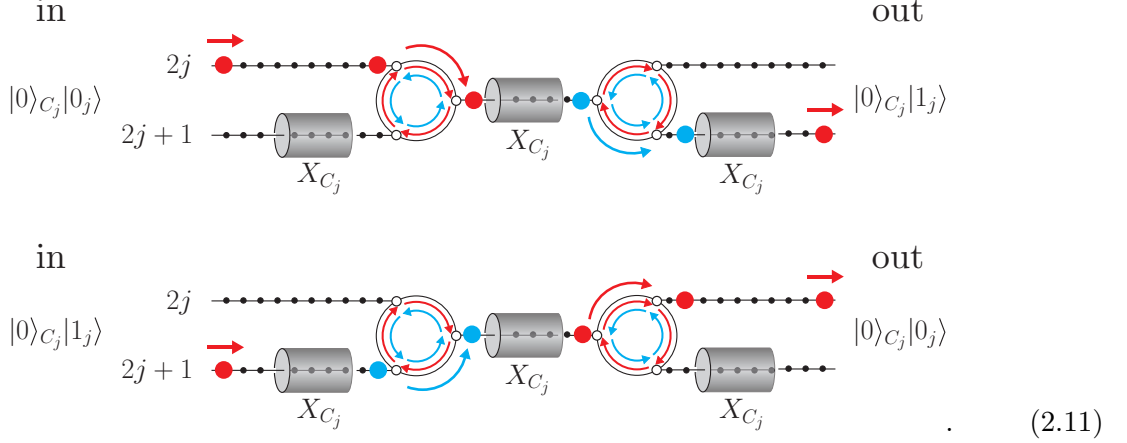
For the spin-1/2 fermionic quantum walks, the operator $R_y(\theta)$ (resp. $R_z(\theta)$) is physically realized by applying a magnetic field H in the direction of y -axis (resp. z -axis) with a specific strength depending on the angle θ . See Fig. 5 in the first paper [1].

Combining the roundabout gate and the gate U_{C_j} , one can construct the single-qubit gate U_j acting on the state $|q_j\rangle$, i.e., $U_j(|0\rangle_{C_j}|q_j\rangle) = |0\rangle_{C_j}(U_j|q_j\rangle)$ as given in [1]:

The diagram shows the construction of the single-qubit gate U_j . It consists of a sequence of components: a roundabout gate, a quantum gate X_{C_j} , another roundabout gate, a quantum gate U_{C_j} , a third roundabout gate, and a final quantum gate X_{C_j} . Two paths, labeled $2j$ and $2j+1$, enter from the left and exit to the right. Path $2j$ starts at an "in" node and ends at an "out" node. Path $2j+1$ starts at an "in" node and ends at an "out" node.

$$\text{Diagram} \quad (2.10)$$

where a red walker is considered as an input walker, i.e., $|0\rangle_{C_j}|q_j\rangle$. For instance, a walker passing through the Pauli- X gate X_j is depicted as



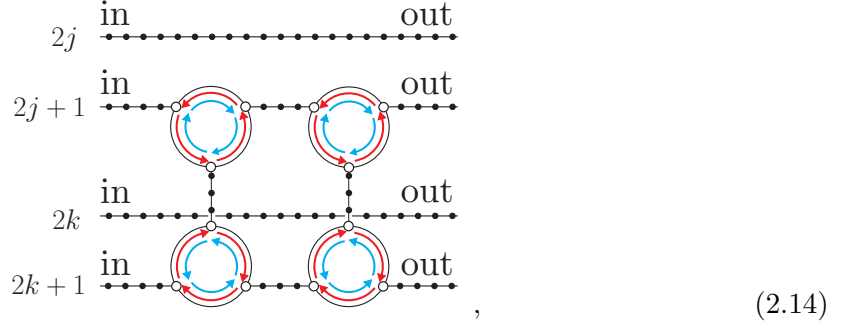
(b) Two-qubit gates Any arbitrary quantum gate can be implemented by a proper combination of single-qubit gates described above and the CNOT gate [2, 50]. The CNOT gate CX_{jk} acting non-trivially on $|q_j\rangle \otimes |q_k\rangle$ is decomposed to

$$CX_{jk} = H_k CP_{jk} H_k, \quad (2.12)$$

where $H_k (= iR_y(\pi/2)_k R_z(\pi)_k)$ is the Hadamard gate acting on $|q_k\rangle$, which is achieved by setting $U_{C_k} = H_{C_k}$ in (2.10). CP_{jk} is a controlled phase gate

$$CP_{jk} = \begin{pmatrix} 1 & 0 & 0 & 0 \\ 0 & 1 & 0 & 0 \\ 0 & 0 & 1 & 0 \\ 0 & 0 & 0 & -1 \end{pmatrix}_{jk}, \quad (2.13)$$

which is physically realized by the scattering of two walkers with the same internal state on an infinite path [1]. (See Sec. 4 in [1] for another controlled phase gate):



where the input state is assumed to be $(|0\rangle_{C_k}|q_k\rangle) \otimes (|0\rangle_{C_j}|q_j\rangle)$.

3 Physical implementation of qRAM

Now we describe an implementation of the qRAM that realizes an algorithm formulated in [49]. Let us explain the details in the order of (i) the routing scheme \mathcal{F} , (ii) the querying

scheme \mathcal{Q} and (iii) the output scheme \mathcal{F}^\dagger . Our qRAM architecture is implemented by these schemes:

$$\text{qRAM} = \mathcal{F}^\dagger \mathcal{Q} \mathcal{F}. \quad (3.1)$$

(i) Routing scheme \mathcal{F} The routing scheme is a scheme to deliver the $(n + m)$ quantum walkers (in superposition) to the desired memory cell(s):

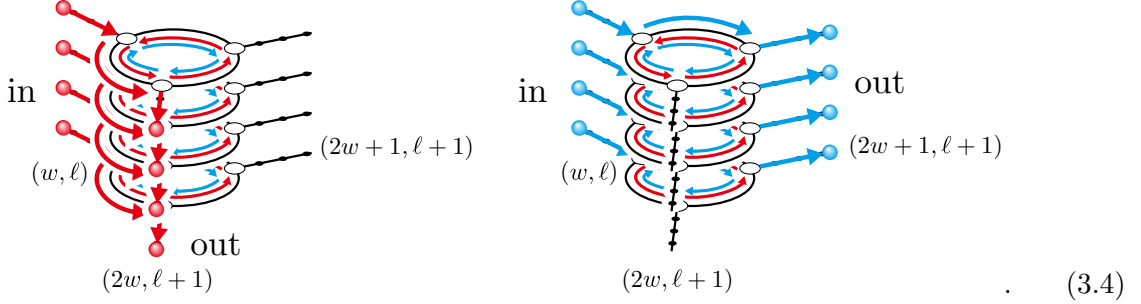
$$\mathcal{F}: \sum_{a \in \mathcal{A}} |a\rangle_A |0, 0\rangle_B |0\rangle_C |0\rangle_D \mapsto \sum_{a \in \mathcal{A}} |a\rangle_A |a, n\rangle_B |0\rangle_C |0\rangle_D. \quad (3.2)$$

The input state

$$\sum_{a \in \mathcal{A}} |a\rangle_A |0, 0\rangle_B |0\rangle_C |0\rangle_D = \sum_{a \in \mathcal{A}} |a_{n-1} \cdots a_0\rangle_A |0, 0\rangle_B |0\rangle_C |0\rangle_D \quad (3.3)$$

is dual-rail encoded into the positions of the $(n + m)$ red quantum walkers at input terminals as in Fig. 2 and Fig. 4. The $(n + m)$ walkers start moving simultaneously toward leaves.

The roundabout gate $U_R^{(1)}$ is installed at each node (w, ℓ) ($0 \leq w \leq 2^\ell - 1$; $0 \leq \ell \leq n - 1$) so that it routes the red walkers (resp. blue walkers) to the left (resp. right) child node $(2w, \ell + 1)$ (resp. $(2w + 1, \ell + 1)$):



Formally this process is given by the operator $\mathcal{R}_{(w, \ell)}$:

$$\mathcal{R}_{(w, \ell)}: |w, \ell\rangle_B \otimes \bigotimes_{j=0}^{n+m-1} |c_j\rangle_{C_j} \mapsto |2w + c, \ell + 1\rangle_B \otimes \bigotimes_{j=0}^{n+m-1} |c_j\rangle_{C_j} \quad (c \in \{0, 1\}). \quad (3.5)$$

The internal states of all the walkers moving to the node (w, ℓ) ($0 \leq w \leq 2^\ell - 1$; $0 \leq \ell \leq n - 1$) must be $|0\rangle_{C_j}$ (resp. $|1\rangle_{C_j}$) ($0 \leq j \leq n + m - 1$) for $a_{n-1-\ell} = 0$ (resp. $a_{n-1-\ell} = 1$), so that the walkers passing through the routers at (w, ℓ) move to the left (resp. right) node. Namely, the positional information of the path traveled by the $(n - 1 - \ell)$ th walker should be encoded to the internal states of all the walkers. This encoding process is formally written by the operator $\mathcal{E}_{(w, \ell)}$ ($0 \leq \ell \leq n - 1$):

$$\mathcal{E}_{(w, \ell)}: \bigotimes_{j=0}^{n-1} |a_j\rangle_{A_j} \otimes \bigotimes_{j=0}^{n+m-1} |w \bmod 2\rangle_{C_j} \mapsto \bigotimes_{j=0}^{n-1} |a_j\rangle_{A_j} \otimes \bigotimes_{j=0}^{n+m-1} |a_{n-1-\ell}\rangle_{C_j}. \quad (3.6)$$

As shown immediately below, the operator $\mathcal{E}_{(w, \ell)}$ is achieved by a CNOT gate $CX_{A_j C_j}$ ($0 \leq j \leq n - 1$):

$$CX_{A_j C_j}: |a_j\rangle_{A_j} \otimes |c_j\rangle_{C_j} \mapsto |a_j\rangle_{A_j} \otimes (\delta_{a_j, 0} |c_j\rangle_{C_j} + \delta_{a_j, 1} X_{C_j} |c_j\rangle_{C_j}), \quad (3.7)$$

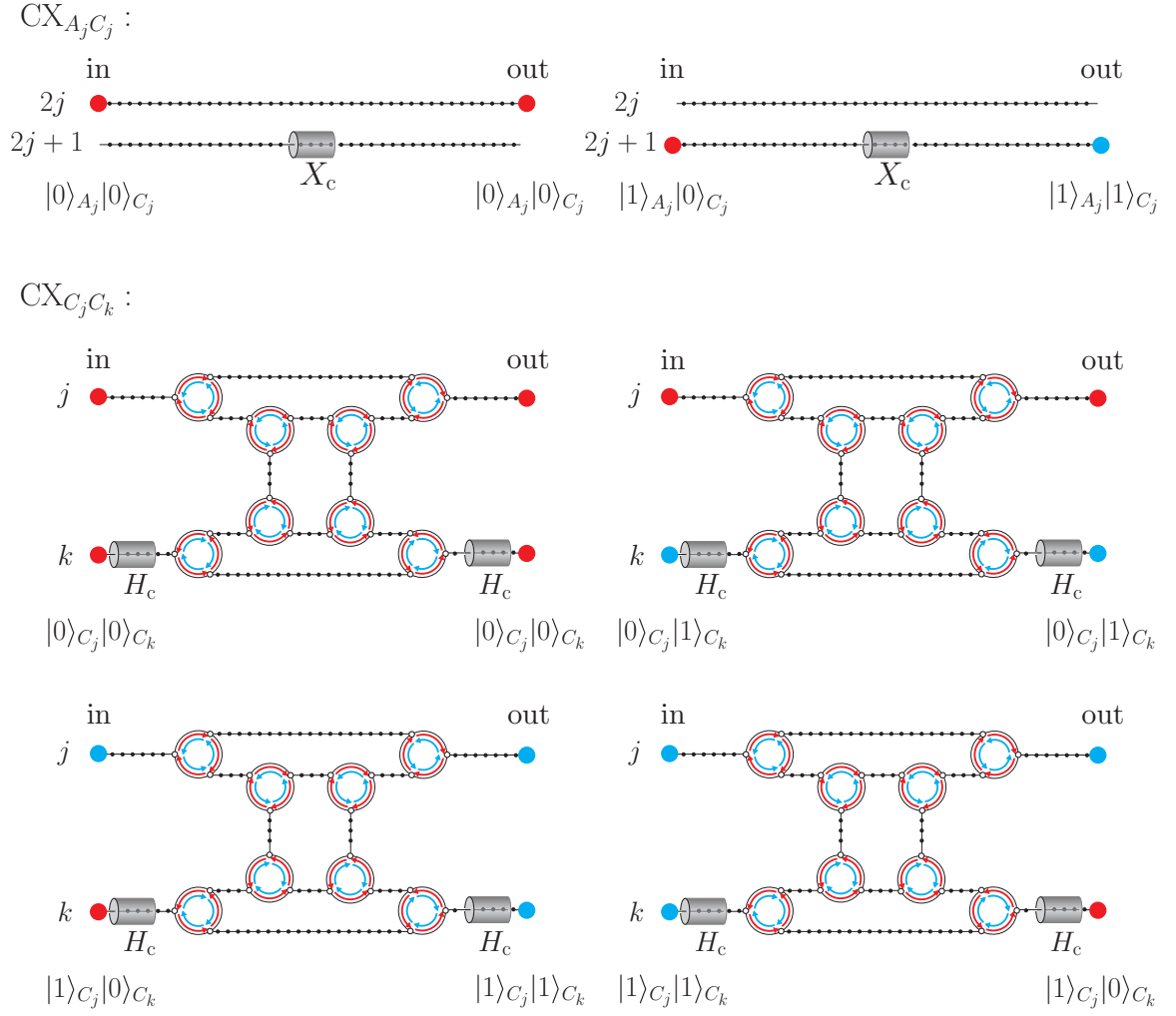


Figure 5: A schematic description of the output states through the gates $CX_{A_j C_j}$ and $CX_{C_j C_k}$ and the corresponding input states.

walker as $|a_{n-1-\ell}\rangle_{C_{n-1-\ell}}$, and $\mathcal{E}_\ell^{(k+1|k)}$ is constructed by

$$\begin{aligned}\mathcal{E}_\ell^{(1|0)} &= [r, r + 2^{p-1}], \\ \mathcal{E}_\ell^{(k+1|k)} &= \prod_{s=0}^{2^{k-1}-1} [r - s2^{p-k}, r - s2^{p-k} - 2^{p-k-1}] \\ &\quad \times [r + 2^{p-1} - s2^{p-k}, r + 2^{p-1} - s2^{p-k} - 2^{p-k-1}] \quad (k \geq 1).\end{aligned}\quad (3.15)$$

Here, $r := n - 1 - \ell$ and we have used the abbreviation

$$[j, k] := \text{CX}_{C_j C_k}, \quad j, k \in \mathbb{Z}/(n+m)\mathbb{Z} \quad (3.16)$$

to simplify the notation. This process may be intuitively understood by the graphical representation as in Fig. 6. Note here that the colors of the walkers are mixed only during this encoding process, otherwise all they are set to either red or blue. Thus, the quantum walkers appropriately move to the paths connecting two nodes (w, ℓ) and $(2w + a_{n-1-\ell}, \ell + 1)$ ($0 \leq w \leq 2^\ell - 1$; $0 \leq \ell \leq n - 1$) by

$$\begin{aligned}\mathcal{F}^{(\ell+1|\ell)} &:= \sum_{w=0}^{2^\ell-1} \mathcal{R}_{(w,\ell)} \mathcal{E}_{(w,\ell)}, \\ \mathcal{F}^{(\ell+1|\ell)} &: |a\rangle_A |w, \ell\rangle_B \otimes \bigotimes_{j=0}^{n+m-1} |a_{n-\ell}\rangle_{C_j} \otimes |0\rangle_D \\ &\mapsto |a\rangle_A |2w + a_{n-1-\ell}, \ell + 1\rangle_B \otimes \bigotimes_{j=0}^{n+m-1} |a_{n-1-\ell}\rangle_{C_j} \otimes |0\rangle_D,\end{aligned}\quad (3.17)$$

where $a_n := 0$. Recursively applying $\mathcal{F}^{(\ell+1|\ell)}$ to the walkers that started moving toward (w, ℓ) from its parent node and finally resetting the colors of the walkers to red, namely, performing the operator

$$\mathcal{F} = \sum_{w=0}^{2^n-1} \mathcal{X}_{(w,n)} \mathcal{F}^{(n|n-1)} \dots \mathcal{F}^{(2|1)} \mathcal{F}^{(1|0)}, \quad (3.18)$$

we properly deliver the walkers (in superposition) to the designated memory cells, as given by (3.2). The depth of the circuit required for the routing scheme is $O(np) = O(n \log(n+m))$.

(ii) Querying scheme \mathcal{Q} The querying scheme \mathcal{Q} is a scheme that loads the data $x^{(a)}$ stored in the memory cell at the address a :

$$\mathcal{Q}: \sum_{a \in \mathcal{A}} |a\rangle_A |a, n\rangle_B |0\rangle_C |0\rangle_D \mapsto \sum_{a \in \mathcal{A}} |a\rangle_A |a, n\rangle_B |0\rangle_C |x^{(a)}\rangle_D, \quad (3.19)$$

which is formally realized by

$$\mathcal{Q} = \sum_{a \in \mathcal{A}} |a, n\rangle \langle a, n|_B \otimes \bigotimes_{i=0}^{m-1} (X_{D_i})^{x_i^{(a)}}. \quad (3.20)$$

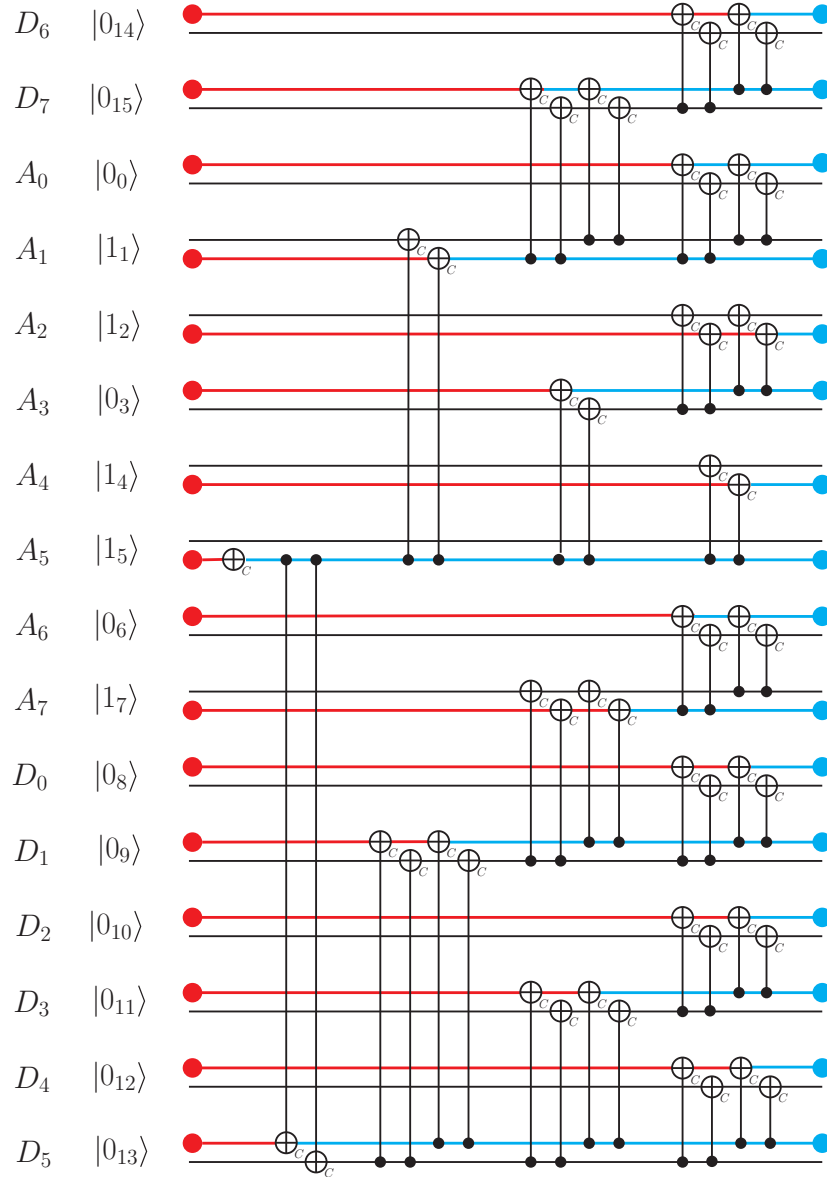


Figure 6: A pictorial representation of the action of $\mathcal{E}_{(w,\ell)}$ defined by (3.14) (see also (3.6)) for $w \in 2\mathbb{Z}$, $\ell = 2$, $n = 8$, $m = 8$, $p = \log_2(n + m) = 4$, $|10110110\rangle_A$ and $|00000000\rangle_D$. After $O(p)$ steps, the positional information $|a_{n-1-\ell}\rangle_{A_{n-1-\ell}} = |1\rangle_{A_5}$ is encoded to the colors of all the walkers: $\bigotimes_{j=0}^{15} |0\rangle_{C_j} \mapsto \bigotimes_{j=0}^{15} |1\rangle_{C_j}$. The number of devices necessary for the processing is $O(n + m)$. Note that the colors of the walkers are mixed only during this encoding process, otherwise all they are set to either red or blue.

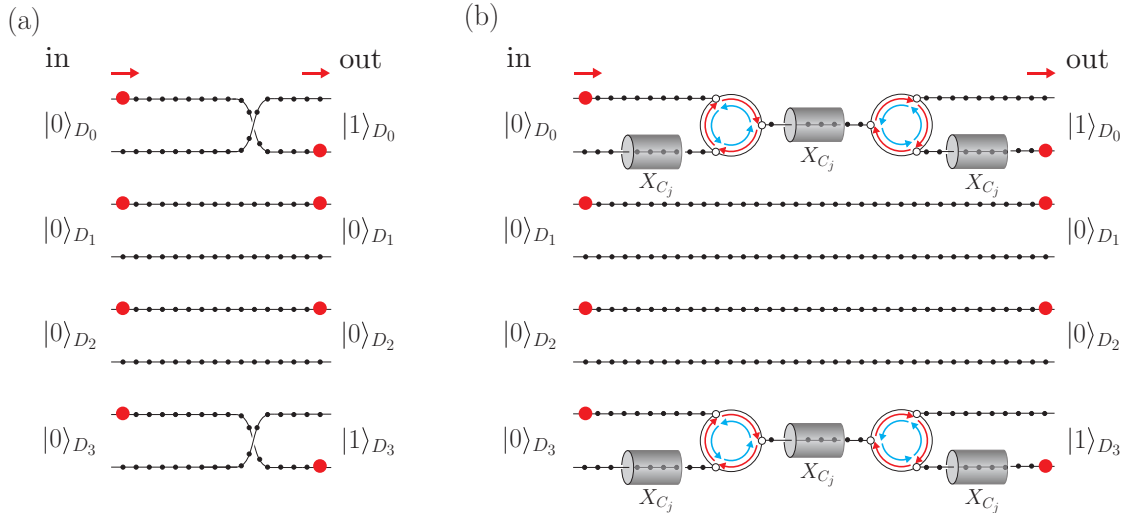


Figure 7: A pictorial representation of the querying scheme (3.19) for $|0000\rangle_D \mapsto |1001\rangle_D$, which can be achieved by (a) exchanging paths or (b) placing the Pauli-X gates.

In our architecture, this scheme is implemented by simply exchanging the appropriate paths in the data register or alternatively by placing the Pauli-X gates (see (2.10)), as pictorially shown in Fig. 7.

(iii) Output scheme \mathcal{F}^\dagger The output scheme is a procedure to retrieve the data in superposition. In the current approach, this scheme is achieved by just applying the reverse operation of the routing scheme, i.e.,

$$\mathcal{F}^\dagger: \sum_{a \in \mathcal{A}} |a\rangle_A |a, n\rangle_B |0\rangle_C |x^{(a)}\rangle_D \mapsto \sum_{a \in \mathcal{A}} |a\rangle_A |0, 0\rangle_B |0\rangle_C |x^{(a)}\rangle_D. \quad (3.21)$$

As shown in Fig. 4, the scheme can be implemented simply by arranging all devices used in the routing scheme so that their positions are perfect mirror images across the memory cells (without changing the direction of the arrows on the roundabout gates).

In summary, the present architecture processes 2^n m -qubit data in $O(n \log(n+m))$ steps, which requires $O(n+m)$ qubit resources and $O((n+m)2^n)$ quantum devices. Table 1 compares the number of computational steps and quantum resources required for the present qRAM architecture and the original bucket-brigade architecture. Compared to the original bucket-brigade qRAM, the advantages of our architecture are that it requires fewer computation steps and qubit resources and does not require time-dependent control. On the other hand, the trade-off for these advantages is that it requires more space and quantum gates, as shown in Figs. 4 and 6.

4 Some modification of routing scheme

By definition (1.2) of qRAM, the address information in superposition, namely, $\sum_a |a\rangle_A$, is prepared beforehand, with no mention of how it is actually constructed. Here, we propose

method	#computational steps	#qubits	#quantum gates
quantum walk	$O(n \log(n+m))$	$O(n+m)$	$O((n+m)2^n)$
bucket-brigade [39, 40]	$O(n^2 + nm)$	$O(2^n + m)$	$O(2^n)$

Table 1: Comparison of the number of computational steps and quantum resources required for the present method and the original bucket-brigade method.

an alternative qRAM architecture that transforms a trivial state into a superposition of information stored in the desired memory cells:

$$\widetilde{\text{qRAM}}: |0\rangle_A |0, 0\rangle_B |0\rangle_C |0\rangle_D \mapsto \frac{1}{\sqrt{|\mathcal{A}|}} \sum_{a \in \mathcal{A}} |a\rangle_A |0, 0\rangle_B |0\rangle_C |x^{(a)}\rangle_D \quad (4.1)$$

(cf. eq. (2.4)), which is accomplished by modifying the routing and querying scheme slightly. Note that, in (4.1), the normalization factor $1/\sqrt{|\mathcal{A}|}$ is written down explicitly to improve the perspective of the discussion here.

First we construct the following routing scheme $\widetilde{\mathcal{F}}$:

$$\widetilde{\mathcal{F}}: |0\rangle_A |0, 0\rangle_B |0\rangle_C |0\rangle_D \mapsto \frac{1}{\sqrt{|\mathcal{A}|}} \sum_{a \in \mathcal{A}} |0\rangle_A |a, n\rangle_B |0\rangle_C |0\rangle_D \quad (4.2)$$

(cf. (3.2)). Note that, in this routing scheme $\widetilde{\mathcal{F}}$, the address information is *not* encoded in the address state, which actually remains $|0\rangle_A$ during the routing. Instead, to deliver the $n+m$ walkers to the memory cells at \mathcal{A} , the Hadamard-like gates are appropriately placed in the first binary tree on the top sheet, where the 0th walker travels. Let $l_{(w,\ell)}$ (resp. $r_{(w,\ell)}$) ($0 \leq w \leq 2^\ell - 1$, $0 \leq \ell \leq n-1$) be the number of designated memory cells whose ancestor is the left child node $(2w, \ell+1)$ (resp. right child node $(2w+1, \ell+1)$) of (w, ℓ) . See Fig. 8 for a simple example. Then, we define the Hadamard-like gate $\mathcal{H}_{(w,\ell)}$ acting on the internal state of the 0th walker that moves to the node (w, ℓ) from its parent node:

$$\mathcal{H}_{(w,\ell)} := \frac{1}{\sqrt{l_{(w,\ell)} + r_{(w,\ell)}}} \begin{pmatrix} \sqrt{l_{(w,\ell)}} & \sqrt{r_{(w,\ell)}} \\ \sqrt{r_{(w,\ell)}} & -\sqrt{l_{(w,\ell)}} \end{pmatrix}_{C_0}, \quad (4.3)$$

which is given by $e^{i\theta} R_y(\theta) R_z(\pi)$ for $\theta = 2 \tan^{-1}(\sqrt{r_{(w,\ell)}/l_{(w,\ell)}})$ and is reduced to the standard Hadamard gate if $l_{(w,\ell)} = r_{(w,\ell)} = 1$ ($\theta = \pi/2$). Using this gate with $\mathcal{R}_{(w,\ell)}$, $\mathcal{X}_{(w,\ell)}$ defined in (3.5) and (3.6), we can actually realize $\widetilde{\mathcal{F}}$:

$$\widetilde{\mathcal{F}} = \sum_{w=0}^{2^n-1} \mathcal{X}_{(w,n)} \widetilde{\mathcal{F}}^{(n|n-1)} \dots \widetilde{\mathcal{F}}^{(2|1)} \widetilde{\mathcal{F}}^{(1|0)}, \quad \widetilde{\mathcal{F}}^{(\ell+1|\ell)} := \sum_{w=0}^{2^\ell-1} \mathcal{R}_{(w,\ell)} \widetilde{\mathcal{E}}_{n-1} \mathcal{H}_{(w,\ell)} \mathcal{X}_{(w,\ell)}, \quad (4.4)$$

where $\widetilde{\mathcal{E}}_\ell$ is defined by slightly modifying \mathcal{E}_ℓ (eq. (3.14)) as

$$\widetilde{\mathcal{E}}_\ell := \mathcal{E}_\ell^{(p|p-1)} \dots \mathcal{E}_\ell^{(2|1)} \mathcal{E}_\ell^{(1|0)}. \quad (4.5)$$

Namely, $\widetilde{\mathcal{E}}_{n-1}$ entangles the internal states of the 0th walker with those of the other walkers:

$$\widetilde{\mathcal{E}}_{n-1}: \sum_c |c\rangle_{C_0} \bigotimes_{j=1}^{n+m-1} |0\rangle_{C_j} \mapsto \sum_c \bigotimes_{j=0}^{n+m-1} |c\rangle_{C_j} \quad (c \in \{0, 1\}). \quad (4.6)$$

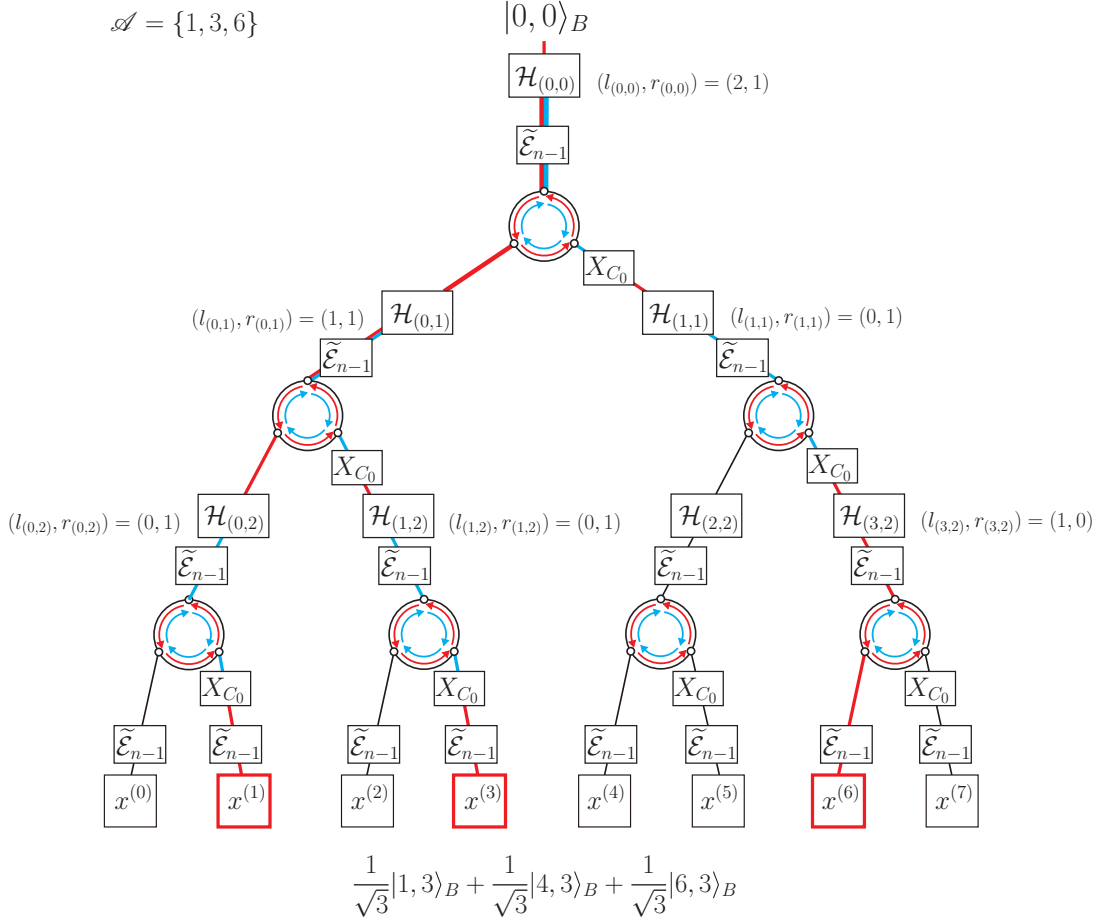


Figure 8: A graphical representation of the modified routing scheme $\tilde{\mathcal{F}}$ defined in (4.2) on the top sheet for $\mathcal{A} = \{1, 3, 6\} = \{001, 011, 110\}$. On the top sheet, the Hadamard-like gate $\mathcal{H}_{(w,\ell)}$ (eq. (4.3)) is equipped on each pass to the node (w, ℓ) ($0 \leq w \leq 2^\ell - 1$, $0 \leq \ell \leq n - 1 = 2$). The internal state generated by passing through $\mathcal{H}_{(w,\ell)}$ is entangled with that of each walker by the gate $\tilde{\mathcal{E}}_{n-1}$.

In Fig. 8, we pictorially show an example of the modified routing scheme on the top sheet.

To properly retrieve the walkers loaded with the data using output scheme \mathcal{F}^\dagger , the address information $|a\rangle_A$ must be encoded in the positions of the quantum walkers. Note that once the data have been loaded, it is no longer possible to retrieve the walkers using $\widetilde{\mathcal{F}}^\dagger$. The querying scheme $\widetilde{\mathcal{Q}}$ corresponding to (3.19) is modified to encode the data as well as the address of the cell where the data is stored:

$$\widetilde{\mathcal{Q}}: \frac{1}{\sqrt{|\mathcal{A}|}} \sum_{a \in \mathcal{A}} |0\rangle_A |a, n\rangle_B |0\rangle_C |0\rangle_D \mapsto \frac{1}{\sqrt{|\mathcal{A}|}} \sum_{a \in \mathcal{A}} |a\rangle_A |a, n\rangle_B |0\rangle_C |x^{(a)}\rangle_D. \quad (4.7)$$

Explicitly it reads

$$\widetilde{\mathcal{Q}} = \sum_{a \in \mathcal{A}} |a, n\rangle \langle a, n|_B \otimes \bigotimes_{i=0}^{n-1} (X_{A_i})^{a_i} \otimes \bigotimes_{i=0}^{m-1} (X_{D_i})^{x_i^{(a)}}, \quad (4.8)$$

which is accomplished by exchanging the specified paths in the address and data register, or alternatively by placing the Pauli-X gates, as explained in the previous section.

Finally applying the output scheme \mathcal{F}^\dagger defined in (3.21), we obtain the desired qRAM architecture (4.1) in the form

$$\widetilde{\text{qRAM}} = \mathcal{F}^\dagger \widetilde{\mathcal{Q}} \mathcal{F}. \quad (4.9)$$

5 Summary and discussion

A qRAM (2.4) or (4.1) has been physically realized by combinations of several elementary quantum devices, including the roundabout gate (2.6) developed in the first paper [1] in this series. 2^n m -qubit information can be retrieved in superposition by simply passing the $n + m$ quantum walkers through the perfect binary trees, as schematically shown in Fig. 4. The advantages of the present qRAM architecture compared to the original bucket-brigade qRAM are summarized as follows: (i) The procedure is completely parallelized without using any ancilla qubit. The 2^n m -qubit information can be retrieved after $O(n \log(n + m))$ steps. The qubit resources and the quantum gates required for the processing are $O(n + m)$ and $O(2^n(n + m))$. (ii) The walkers do not entangle with any device on the binary trees, which promises to reduce the cost of maintaining quantum coherence. (iii) Our qRAM architecture is free from any time-dependent control. In other words, information in quantum superposition can be composed by just passing the walkers through the binary trees. On the other hand, the trade-off for these advantages is that it requires more space and quantum gates.

Finally, let us discuss how to generalize the present architecture to be able to process quantum information (i.e. information stored in the cell consists of a superposition of states). In the querying scheme described in Sec. 3, m -bit classical information stored in a memory cell can be directly copied to an m -qubit state of the data register (see (3.19) and (3.20)), which can be achieved by exchanging the appropriate paths in the data register or by placing the Pauli-X gates. For the quantum case, however, quantum information can not be replicated due to the no-cloning theorem [51, 52]. Instead, by a swap gate, the quantum information can be transferred to the state in the data register. In our architecture, m -qubit quantum information stored in the cell at address a can be represented as the internal states of m quantum walkers, each moving in a circle, as shown in Fig. 9. (This may be realized by

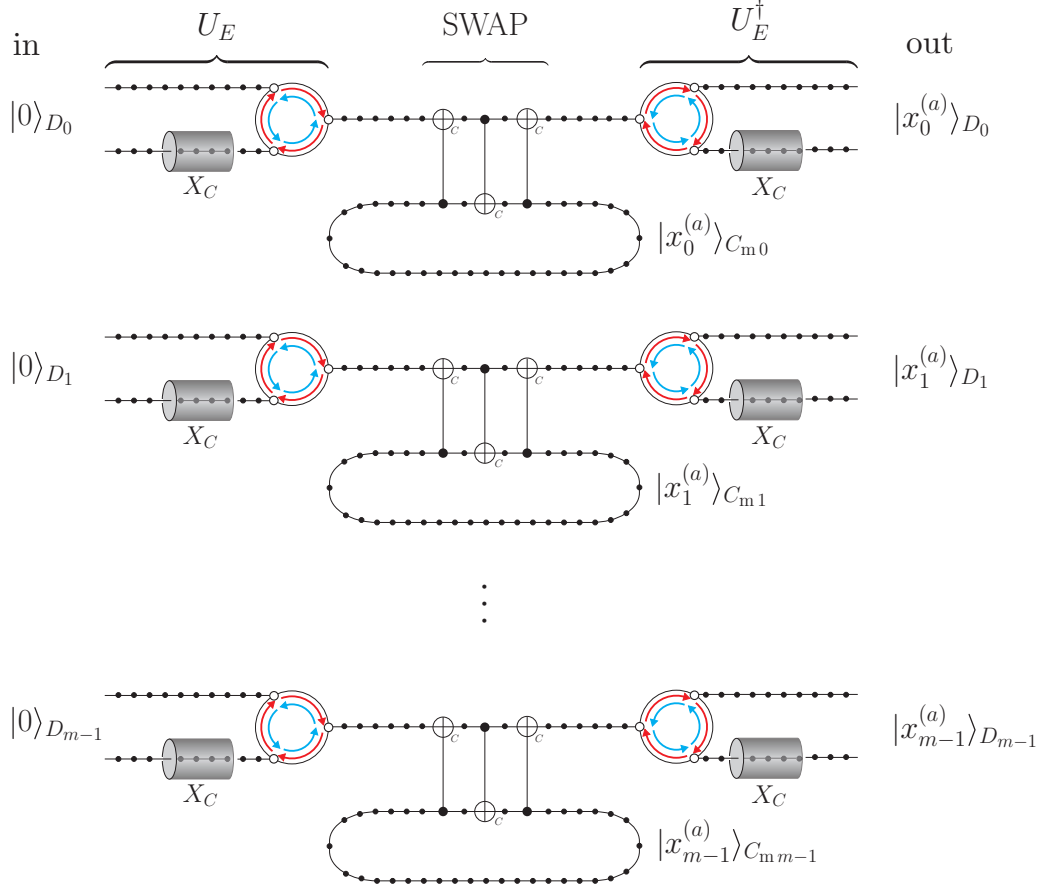


Figure 9: A physical realization of the process (5.1). Quantum information is represented as the internal states of quantum walkers, which can be stored in the memory cell using a *quantum memory* developed in the first paper [1]. The information stored in the memory cell is transferred by the encoder/decoder U_E/U_E^\dagger and the swap gate consisting of the CNOT gates defined in (3.10).

a *quantum memory* developed in Sec. 6 in the first paper [1]). Explicitly, it is expressed as $\sum_x |x^{(a)}\rangle_{C_m}$, where the index C_m stands for the colors of the quantum walkers in the memory cell. As shown in Fig. 9, combining an encoder U_E (see eq. (4.2) in the first paper [1] for a precise definition), which encodes the position of the quantum walker into the internal state of the walker, and the swap gate consisting of the three CNOT gates $CX_{C_j C_k}$ in (3.10), we can correctly transfer the quantum information in the memory cell to the data register:

$$\sum_x |x^{(a)}\rangle_{C_m} \mapsto \sum_x |x^{(a)}\rangle_D. \quad (5.1)$$

Combining the model of universal quantum computation achieved in the first paper [1] with the current qRAM architecture is expected to enable efficient processing of quantum information such as the quantum phase estimation [3], Grover's algorithm for searching unsorted databases [7], and the quantum version of fast Fourier transform [53].

Acknowledgment

The present work was partially supported by Grant-in-Aid for Scientific Research (C) No. 20K03793 from the Japan Society for the Promotion of Science.

References

- [1] Ryo Asaka, Kazumitsu Sakai, and Ryoko Yahagi. Two-level quantum walkers on directed graphs I: Universal quantum computing. *arXiv preprint arXiv:2112.08119*, 2021.
- [2] Michael A Nielsen and Isaac Chuang. Quantum computation and quantum information, 2002.
- [3] Peter W Shor. Algorithms for quantum computation: discrete logarithms and factoring. In *Proceedings 35th annual symposium on foundations of computer science*, pages 124–134. IEEE, 1994.
- [4] A Yu Kitaev. Quantum measurements and the abelian stabilizer problem. *arXiv preprint quant-ph/9511026*, 1995.
- [5] Gilles Brassard and Peter Hoyer. An exact quantum polynomial-time algorithm for simon’s problem. In *Proceedings of the Fifth Israeli Symposium on Theory of Computing and Systems*, pages 12–23. IEEE, 1997.
- [6] Gilles Brassard, Peter Hoyer, Michele Mosca, and Alain Tapp. Quantum amplitude amplification and estimation. *Contemporary Mathematics*, 305:53–74, 2002.
- [7] Lov K Grover. A fast quantum mechanical algorithm for database search. In *Proceedings of the twenty-eighth annual ACM symposium on Theory of computing*, pages 212–219, 1996.
- [8] Lov K Grover. Quantum computers can search rapidly by using almost any transformation. *Physical Review Letters*, 80(19):4329, 1998.
- [9] Richard P Feynman. Simulating physics with computers. In *Feynman and computation*, pages 133–153. CRC Press, 2018.
- [10] Seth Lloyd. Universal quantum simulators. *Science*, pages 1073–1078, 1996.
- [11] Dominic W Berry, Graeme Ahokas, Richard Cleve, and Barry C Sanders. Efficient quantum algorithms for simulating sparse hamiltonians. *Communications in Mathematical Physics*, 270(2):359–371, 2007.
- [12] Dominic W Berry and Andrew M Childs. Black-box hamiltonian simulation and unitary implementation. *Quantum Information and Computation*, 12(1-2):29–62, 2012.
- [13] Dominic W Berry, Andrew M Childs, and Robin Kothari. Hamiltonian simulation with nearly optimal dependence on all parameters. In *2015 IEEE 56th Annual Symposium on Foundations of Computer Science*, pages 792–809. IEEE, 2015.

- [14] Dominic W Berry, Andrew M Childs, Richard Cleve, Robin Kothari, and Rolando D Somma. Simulating hamiltonian dynamics with a truncated taylor series. *Physical review letters*, 114(9):090502, 2015.
- [15] Guang Hao Low and Isaac L Chuang. Optimal hamiltonian simulation by quantum signal processing. *Physical review letters*, 118(1):010501, 2017.
- [16] Andrew M Childs, Dmitri Maslov, Yunseong Nam, Neil J Ross, and Yuan Su. Toward the first quantum simulation with quantum speedup. *Proceedings of the National Academy of Sciences*, 115(38):9456–9461, 2018.
- [17] Guang Hao Low and Isaac L Chuang. Hamiltonian simulation by qubitization. *Quantum*, 3:163, 2019.
- [18] Bela Bauer, Sergey Bravyi, Mario Motta, and Garnet Kin-Lic Chan. Quantum algorithms for quantum chemistry and quantum materials science. *Chemical Reviews*, 120(22):12685–12717, 2020.
- [19] George F Viamontes, Igor L Markov, and John P Hayes. Is quantum search practical? *Computing in science & engineering*, 7(3):62–70, 2005.
- [20] Seth Lloyd, Masoud Mohseni, and Patrick Rebentrost. Quantum algorithms for supervised and unsupervised machine learning. *arXiv preprint arXiv:1307.0411*, 2013.
- [21] Patrick Rebentrost, Masoud Mohseni, and Seth Lloyd. Quantum support vector machine for big data classification. *Physical review letters*, 113(13):130503, 2014.
- [22] Peter Wittek. *Quantum machine learning: what quantum computing means to data mining*. Academic Press, 2014.
- [23] Anupam Prakash. *Quantum algorithms for linear algebra and machine learning*. University of California, Berkeley, 2014.
- [24] Maria Schuld, Ilya Sinayskiy, and Francesco Petruccione. An introduction to quantum machine learning. *Contemporary Physics*, 56(2):172–185, 2015.
- [25] Jeremy Adcock, Euan Allen, Matthew Day, Stefan Frick, Janna Hinchliff, Mack Johnson, Sam Morley-Short, Sam Pallister, Alasdair Price, and Stasja Stanisic. Advances in quantum machine learning. *arXiv preprint arXiv:1512.02900*, 2015.
- [26] Jacob Biamonte, Peter Wittek, Nicola Pancotti, Patrick Rebentrost, Nathan Wiebe, and Seth Lloyd. Quantum machine learning. *Nature*, 549(7671):195–202, 2017.
- [27] Maria Schuld, Mark Fingerhuth, and Francesco Petruccione. Implementing a distance-based classifier with a quantum interference circuit. *EPL (Europhysics Letters)*, 119(6):60002, 2017.
- [28] Vedran Dunjko and Hans J Briegel. Machine learning & artificial intelligence in the quantum domain: a review of recent progress. *Reports on Progress in Physics*, 81(7):074001, 2018.

- [29] Carlo Ciliberto, Mark Herbster, Alessandro Davide Ialongo, Massimiliano Pontil, Andrea Rocchetto, Simone Severini, and Leonard Wossnig. Quantum machine learning: a classical perspective. *Proceedings of the Royal Society A: Mathematical, Physical and Engineering Sciences*, 474(2209):20170551, 2018.
- [30] Iordanis Kerenidis, Jonas Landman, Alessandro Luongo, and Anupam Prakash. q-means: A quantum algorithm for unsupervised machine learning. *arXiv preprint arXiv:1812.03584*, 2018.
- [31] Xun Gao, Z-Y Zhang, and L-M Duan. A quantum machine learning algorithm based on generative models. *Science advances*, 4(12):eaat9004, 2018.
- [32] Maria Schuld and Nathan Killoran. Quantum machine learning in feature hilbert spaces. *Physical review letters*, 122(4):040504, 2019.
- [33] Jeongho Bang, Arijit Dutta, Seung-Woo Lee, and Jaewan Kim. Optimal usage of quantum random access memory in quantum machine learning. *Physical Review A*, 99(1):012326, 2019.
- [34] Somayeh Bakhtiari Ramezani, Alexander Sommers, Harish Kumar Manchukonda, Shahram Rahimi, and Amin Amirlatifi. Machine learning algorithms in quantum computing: A survey. In *2020 International Joint Conference on Neural Networks (IJCNN)*, pages 1–8. IEEE, 2020.
- [35] Yao Zhang and Qiang Ni. Recent advances in quantum machine learning. *Quantum Engineering*, 2(1):e34, 2020.
- [36] Xu Zhou and Daowen Qiu. Blind quantum machine learning based on quantum circuit model. *Quantum Information Processing*, 20(11):1–28, 2021.
- [37] Nimish Mishra, Manik Kapil, Hemant Rakesh, Amit Anand, Nilima Mishra, Aakash Warke, Soumya Sarkar, Sanchayan Dutta, Sabhyata Gupta, Aditya Prasad Dash, et al. Quantum machine learning: A review and current status. *Data Management, Analytics and Innovation*, pages 101–145, 2021.
- [38] Weiwen Jiang, Jinjun Xiong, and Yiyu Shi. When machine learning meets quantum computers: A case study. In *2021 26th Asia and South Pacific Design Automation Conference (ASP-DAC)*, pages 593–598. IEEE, 2021.
- [39] Vittorio Giovannetti, Seth Lloyd, and Lorenzo Maccone. Quantum random access memory. *Physical review letters*, 100(16):160501, 2008.
- [40] Vittorio Giovannetti, Seth Lloyd, and Lorenzo Maccone. Architectures for a quantum random access memory. *Physical Review A*, 78(5):052310, 2008.
- [41] Connor T Hann, Gideon Lee, SM Girvin, and Liang Jiang. Resilience of quantum random access memory to generic noise. *PRX Quantum*, 2(2):020311, 2021.
- [42] Alexandru Paler, Oumarou Oumarou, and Robert Basmadjian. Parallelizing the queries in a bucket-brigade quantum random access memory. *Physical Review A*, 102(3):032608, 2020.

- [43] Srinivasan Arunachalam, Vlad Gheorghiu, Tomas Jochym-O'Connor, Michele Mosca, and Priyaa Varshinee Srinivasan. On the robustness of bucket brigade quantum ram. *New Journal of Physics*, 17(12):123010, 2015.
- [44] Olivia Di Matteo, Vlad Gheorghiu, and Michele Mosca. Fault-tolerant resource estimation of quantum random-access memories. *IEEE Transactions on Quantum Engineering*, 1:1–13, 2020.
- [45] Fang-Yu Hong, Yang Xiang, Zhi-Yan Zhu, Li-zhen Jiang, and Liang-neng Wu. Robust quantum random access memory. *Physical Review A*, 86(1):010306, 2012.
- [46] Thi Ha Kyaw, Simone Felicetti, Guillermo Romero, Enrique Solano, and L-C Kwek. Scalable quantum memory in the ultrastrong coupling regime. *Scientific reports*, 5(1):1–5, 2015.
- [47] Connor T Hann, Chang-Ling Zou, Yaxing Zhang, Yiwen Chu, Robert J Schoelkopf, Steven M Girvin, and Liang Jiang. Hardware-efficient quantum random access memory with hybrid quantum acoustic systems. *Physical review letters*, 123(25):250501, 2019.
- [48] K. C. Chen, W. Dai, C. Errando-Herranz, S. Lloyd, and D. Englund. Scalable and high-fidelity quantum random access memory in spin-photon networks. *PRX Quantum*, 2:030319, Aug 2021.
- [49] Ryo Asaka, Kazumitsu Sakai, and Ryoko Yahagi. Quantum random access memory via quantum walk. *Quantum Science and Technology*, 6(3):035004, 2021.
- [50] Colin P Williams. Quantum gates. In *Explorations in Quantum Computing*, pages 51–122. Springer, 2011.
- [51] William K Wootters and Wojciech H Zurek. A single quantum cannot be cloned. *Nature*, 299(5886):802–803, 1982.
- [52] DGBJ Dieks. Communication by epr devices. *Physics Letters A*, 92(6):271–272, 1982.
- [53] Ryo Asaka, Kazumitsu Sakai, and Ryoko Yahagi. Quantum circuit for the fast fourier transform. *Quantum Information Processing*, 19(8):1–20, 2020.